

One-electron scattering rate and normal-state linear- T resistivity of the cuprates

J. M. P. Carmelo

GCEP-Centre of Physics, University of Minho, Campus Gualtar, P-4710-057 Braga, Portugal.

Here we use a description of the electronic correlations contained in the Hubbard model on the square-lattice perturbed by very weak three-dimensional uniaxial anisotropy in terms of the residual interactions of charge c fermions and spin-neutral composite two-spinon $s1$ fermions. Excellent quantitative agreement with the anisotropic linear- ω one-electron scattering rate and normal-state linear- T resistivity observed in experiments on hole-doped cuprates with critical concentrations $x_c \approx 0.05$ and $x_* \approx 0.27$ is achieved. Our results provide strong evidence that the normal-state linear- T resistivity is a manifestation of low-temperature scale-invariant physics.

I. INTRODUCTION

There is evidence of quantum critical behaviour in the cuprate superconductors^{1–5}. Its physical nature and the mechanism underlying the pairing state^{6–9} are not well understood. Here we use a description of the electronic correlations contained in the Hubbard model on the square-lattice^{6,7,10} perturbed by very weak three-dimensional (3D) uniaxial anisotropy in terms of the residual interactions of charge c fermions and spin-neutral composite two-spinon $s1$ fermions^{10–12}. The interplay of the c Fermi line isotropy with the $s1$ band boundary line anisotropy plays a major role in the one-electron scattering properties. Excellent quantitative agreement with the anisotropic linear- ω one-electron scattering rate and normal-state linear- T resistivity observed in experiments on hole-doped cuprates with critical concentrations $x_c \approx 0.05$ and $x_* \approx 0.27$ is achieved. Our results provide strong evidence that the normal-state linear- T resistivity is a manifestation of low-temperature scale-invariant physics near a hole concentration $x_{c2} \approx 0.20 - 0.22$.

Recent experiments on the hole-doped cuprate superconductors^{3,4,9,13–26} impose new severe constraints on the mechanisms responsible for their unusual properties. The above toy model provides the simplest realistic description of the role of correlations effects in these properties. It involves the effective transfer integrals t and $t_{\perp} \ll t$ and effective on-site repulsion U .

An extended presentation of the results of this manuscript, including needed supplementary information, can be found in Ref.¹¹.

II. THE VIRTUAL-ELECTRON PAIR QUANTUM LIQUID

The virtual-electron pair quantum liquid (VEPQL)¹² describes that toy model electronic correlations in terms of residual $c - s1$ fermion interactions. Unlike the Fermi-liquid quasi-particle momenta^{11,27}, those of the c and $s1$ fermions are close to good quantum numbers^{10,12}.

The results of Ref.¹² provide strong evidence that for hole concentrations $x \in (x_c, x_*)$ the VEPQL short-range spin order coexists with a long-range d -wave super-

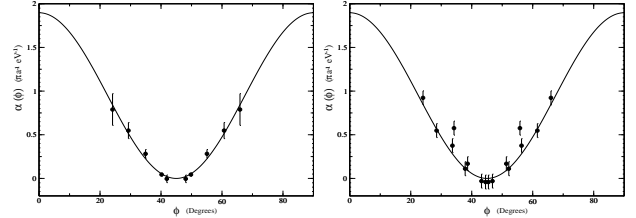


FIG. 1: **The theoretical and LSCO scattering-rate linear- ω coefficient.** The theoretical coefficient $\alpha(\phi)$ given in Ref.¹¹ (solid line) for $x = 0.145$ and the LSCO parameters of the Table I together with the experimental points for the corresponding coefficients $[\alpha_I(\phi) - \alpha_I(\pi/4)]$ and $[\alpha_{II}(\phi) - \alpha_{II}(\pi/4)]$ of Fig. 4 (c) of Ref.²⁰.

conducting order consistent with unconventional superconductivity being mediated by magnetic fluctuations¹³. The *virtual-electron pair* configurations involve one zero-momentum c fermion pair of charge $-2e$ and one spin-singlet two-spin-1/2 spinon $s1$ fermion. The VEPQL predictions achieve an excellent agreement with the cuprates universal properties¹² and consistency with the coexisting two-gap scenario^{9,18,24,25}: A dome-like superconducting energy scale $2|\Omega|$ and pseudogap $2|\Delta|$, over the whole dome $x \in (x_c, x_*)$. Those are the maximum magnitudes of the superconducting virtual-electron pairing energy and spin-singlet spinon pairing energy, respectively.

In the ground state there is no one-to-one correspondence between a c fermion pair and a two-spinon $s1$ fermion: The strong effective coupling of c fermion pairs whose hole momenta \vec{q}^h and $-\vec{q}^h$ belong to an approximately circular $c - sc$ line centered at $-\vec{\pi} = -[\pi, \pi]$, of radius $q^h = |\vec{q}^h| \in (q_{Fc}^h, q_{ec}^h)$ and c fermion energy $|\epsilon_c(q^h)| \in (0, W_{ec})$, results from interactions with well-defined $s1$ fermions. Those have $s1$ band momentum \vec{q} belonging to a corresponding $s1 - sc$ line arc centered at $\vec{0} = [0, 0]$. Here $|\epsilon_c(q_{Fc}^h)| = 0$ and $|\epsilon_c(q_{ec}^h)| = W_{ec}$. For Fermi angles $\phi \in (0, \pi/2)$ a $s1 - sc$ line arc can be labelled either by its nodal momentum absolute value $q_{arc}^N = q_{arc}^N(q^h) \in (q_{ec}^N, q_{Bs1}^N)$ or angular width $2\phi_{arc} \in (0, \pi/2)$ given in Ref.¹¹. $q_{Bs1}^N = q_{Bs1}^N(q_{Fc}^h)$ is the $s1$ band nodal boundary-line momentum^{10,12}, $q_{Fc}^h \approx \sqrt{x}\pi/2$ and $q_{ec}^N = q_{ec}^N(q_{ec}^h)$ and q_{ec}^h are given in that reference. The energy needed for the c fermion strong effective coupling is supplied by the short-range spin correlations through the

c - $s1$ fermion interactions within each virtual-electron pair configuration. Virtual-electron pairs exist in virtual intermediate states of pair-breaking one-electron and spin excitations. Provided that the c fermion effective coupling is strong, virtual-electron pair breaking under one-electron removal excitations gives rise to sharp-feature-line arcs centered at momenta $\pm\vec{\pi} = \pm[\pi, \pi]$ in one-to-one correspondence to the $s1$ - sc -line arcs of its $s1$ fermion. Such sharp-feature-line arcs have angular range $\phi \in (\pi/4 - \phi_{arc}, \pi/4 + \phi_{arc})$, energy $E \approx 2W_{ec}(1 - \sin 2\phi_{arc})$ and well-defined hole momentum $\vec{k}^h = \vec{k} + \vec{\pi}$ and thus exist only for $E < E_1(\phi) = 2W_{ec}(1 - |\cos 2\phi|)$. The macroscopic condensate refers to zero-momentum c fermion pairs whose phases $\theta = \theta_0 + \theta_1$ line up. The fluctuations of θ_0 and θ_1 become large for $x \rightarrow x_c$ and $x \rightarrow x_*$, respectively. The dome x dependence of the critical temperature T_c given in Refs.^{11,12} is fully determined by the interplay of such fluctuations. A pseudogap state with short-range spin order and virtual-electron pair configurations without phase coherence occurs for temperatures $T \in (T_c, T^*)$ where T^* is the pseudogap temperature also given in these references. At $T = 0$ a normal state emerges by application of a magnetic field aligned perpendicular to the planes of magnitude $H \in (H_0, H_{c2})$ for $x \in (x_0, x_{c2})$ and $H \in (H_0, H^*)$ for $x \in (x_{c2}, x_*)$. The fields H_0 , H_{c2} and H^* are given in Refs.^{11,12}.

III. THE ONE-ELECTRON SCATTERING RATE AND NORMAL-STATE LINEAR- T RESISTIVITY OF THE HOLE-DOPED CUPRATES

The main goals of this paper are: i) The study of the one-electron scattering rate and normal-state T -dependent resistivity within the VEPQL; ii) Contributing to the further understanding of the role of scale-invariant physics in the unusual scattering properties of the hole-doped cuprates. The parameters appropriate to $\text{YBa}_2\text{Cu}_3\text{O}_{6+\delta}$ (YBCO 123) and $\text{La}_{2-x}\text{Sr}_x\text{CuO}_4$ (LSCO) found in Ref.¹² are given in Table I.

Our results refer to a range $x \in (x_A, x_{c2})$ for which $V_{Bs1}^\Delta/V_{Fc} \ll 1$ where the $s1$ boundary line and c Fermi velocities are given in Refs.^{11,12} and $x_A \approx x_*/2 = 0.135$. For $x \in (x_{c2}, x_*)$ that condition is also fulfilled but there emerge competing scattering processes difficult to describe in terms of c - $s1$ fermion interactions. Consistently with the validity of our scheme, in Ref.¹¹ it is shown that the VEPQL predictions agree quantitatively with the distribution of the experimental LSCO sharp photoemission spectral features. As predicted, they occur for energies $E(\phi) < E_1(\phi)$ and the corresponding energy, nodal-momentum and sharp-feature line arcs angular ranges agree with the theoretical magnitudes. Such an analysis reveals clear experimental spectral signatures of the VEPQL virtual-electron pairing mechanism. A Fermi's golden rule in terms of the c - $s1$ fermion interactions is then used in Ref.¹¹ to calculate for the parameters of Table I, small $\hbar\omega$ and

system	$U/4t$	t (meV)	Δ_0 (meV)	x_c
YBCO 123	1.525	295	84	0.05
LSCO	1.525	295	42	0.05

TABLE I: The magnitudes of four basic parameters appropriate to YBCO 123 and LSCO within the VEPQL scheme of Ref. [11]. The magnitude of the ratio $U/4t$ given here is set so that the $T = 0$ dome upper critical hole concentration reads $x_* = 0.27$. Those of the effective transfer integral t and energy parameter Δ_0 control the magnitudes of the VEPQL energy scales. The magnitudes of the suppression coefficient $\gamma_d^{min} = 0.95$ for YBCO 123 and $\gamma_d^{min} = 0.82$ for LSCO reached at $x = x_{op} = 0.16$ account for the small effects of superfluid density anisotropy and intrinsic disorder, respectively, on the critical temperature T_c of Eq. (??). They do not play an important role in the quantities studied in the letter. Moreover, the magnitudes $\varepsilon^2 = 6.2 \times 10^{-3}$ for YBCO 123 and $\varepsilon^2 = 3.4 \times 10^{-4}$ for LSCO of the very small 3D uniaxial anisotropy coefficient $\varepsilon^2 \propto t_\perp/t$ defined in Ref.¹² are set so that the $T = 0$ lower dome critical hole concentration reads $x_c \approx 0.05$, as given in this table.

both the normal and superconducting states the one-electron inverse lifetime $\hbar/\tau_{el} \approx \hbar\omega \pi \alpha_{\tau_{el}}$ and scattering rate $\Gamma(\phi, \omega) = 1/[\tau_{el} V_F] \approx \hbar\omega \pi \alpha$. Here V_F is the Fermi velocity, $\alpha_{\tau_{el}} = [\pi/16\sqrt{x x_{op}}](\cos 2\phi)^2$ and $\alpha = (\cos 2\phi)^2/(x 64x_*\sqrt{\pi x_{op}}t)$ where $x_{op} = (x_* + x_c)/2 = 0.16$. (We use units of lattice constant $a = 1$.) As discussed in Ref.¹¹, such small- $\hbar\omega$ expressions are expected to remain valid for approximately $\hbar\omega < E_1(\phi)$. The factor $(\cos 2\phi)^2$ also appears in the anisotropic component of the scattering rate studied in Ref.²⁶ for hole concentrations $x > x_{c2}$. For $x = 0.145$ the use of the Table I LSCO parameters leads to the theoretical coefficient $\alpha(\phi)$ plotted in Fig. 1 (solid line) together with the experimental points of Fig. 4 (c) of Ref.²⁰ for the coefficients $[\alpha_I(\phi) - \alpha_I(\pi/4)]$ and $[\alpha_{II}(\phi) - \alpha_{II}(\pi/4)]$. (The very small $\alpha_I(\pi/4)$ magnitude and small $\alpha_{II}(\pi/4)$ magnitude are related to processes that are not contained in the VEPQL.) An excellent quantitative agreement is obtained between $\alpha(\phi)$ and the experimental points of both $[\alpha_I(\phi) - \alpha_I(\pi/4)]$ and $[\alpha_{II}(\phi) - \alpha_{II}(\pi/4)]$.

In the following we provide strong evidence from agreement between theory and experiments that the linear- T resistivity is indeed a manifestation of normal-state scale-invariant physics. This requires that the T -dependence of the inverse relaxation lifetime derived for finite magnetic field, $x \in (x_A, x_{c2})$ and $\hbar\omega \ll \pi k_B T$ by replacing $\hbar\omega$ by $\pi k_B T$ in the one-electron inverse lifetime $1/\tau_{el}$ and averaging over the Fermi line leads to the observed low- T resistivity. The use in the Appendix A of that procedure leads to the following resistivity expression,

$$\rho(T) \approx \left(\frac{\hbar d_{\parallel}}{te^2}\right) \left(\frac{\pi}{4}\right)^3 \frac{x_*}{x^{3/2}\sqrt{x_{op}}} \pi k_B T. \quad (1)$$

Consistency with the above \hbar/τ_{el} expression validity range $\hbar\omega < E_1(\phi)$ implies that the behaviour (1) remains

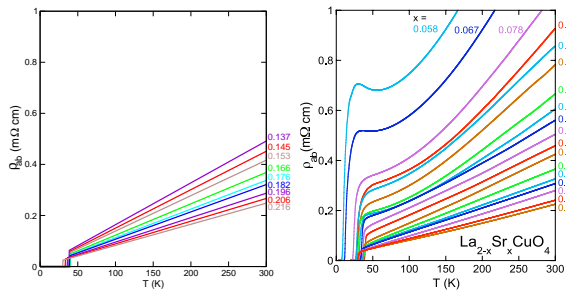


FIG. 2: **Theoretical and LSCO linear- T resistivity.** The T dependence of the resistivity $\rho(T, 0) = \theta(T - T_c)\rho(T)$ with $\rho(T)$ given in Eq. (1) for $x \in (x_A, x_{c2})$ where $x_A \approx 0.135$ and $x_{c2} \approx 0.20 - 0.22$ and the parameter magnitudes of the Table I for LSCO and corresponding experimental curves. Experimental curves figure from Ref.²⁸.

dominant in the normal-state range $T \in (0, T_1)$. Here,

$$T_1 \approx \frac{2}{\pi} \int_0^{\pi/2} d\phi \frac{E_1(\phi)}{k_B} = \frac{(2\pi - 4)W_{ec}}{\pi^2 k_B}. \quad (2)$$

At $x = 0.16$ use of the parameters of the Table I gives $T_1 \approx 554\text{K}$ for LSCO and $T_1 \approx 1107\text{K}$ for YBCO 123. Extrapolation of expression (1) to $H = 0$ leads to $\rho(T, 0) \approx \theta(T - T_c)\rho(T)$ for $T < T_1$. Here the critical low- T resistivity behaviour (1) is masked by the onset of superconductivity at $T = T_c$.

We now compare our theoretical linear- T resistivity with that of LSCO²⁸ and YBCO 123²⁹ for $H = 0$ and T up to 300K. Transport in the b direction has for YBCO 123 contributions from the CuO chains, which render our results unsuitable. In turn, $\rho_a(T, 0) \approx \theta(T - T_c)\rho(T)$ at $H = 0$ for the a direction. $\rho(T, 0)$ and $\rho_a(T, 0)$ are plotted in Figs. 2 and 3 for the Table I parameters for LSCO and YBCO 123, respectively. x is between $x \approx x_A \approx 0.135$ and $x_{c2} \approx 0.20 - 0.22$ for the LSCO theoretical lines of Fig. 2. Fig. 3 for YBCO 123 refers to three x values near x_{op} , expressed in terms of the oxygen content. Comparison of the theoretical curves of Fig. 2 with the LSCO resistivity curves of Ref.²⁸ also shown in the figure confirms an excellent quantitative agreement between theory and experiments for the present range $x \in (x_A, x_{c2})$. In turn, for YBCO 123 our scheme provides a good quantitative description of the experimental curves near x_{op} , for $y = 6.95, 7.00$. The $y = 6.85$ experimental curve of Ref.²⁹ already deviates from the linear- T behaviour. The corresponding effective hole concentration $x_A \approx 0.15$ is for that material consistent with the inequality $x_A \in (0.12, 0.15)$ found in Ref.¹¹. In turn, for $x > x_{c2}$ a competing scattering channel emerges, leading to an additional T^2 -quadratic resistivity contribution^{3,4}.

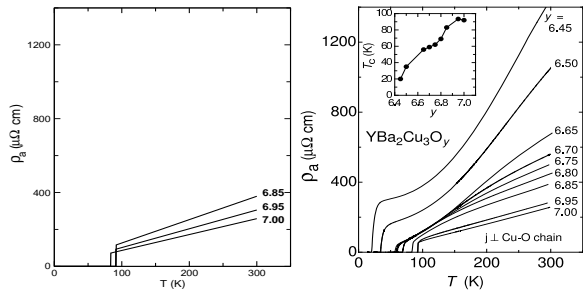


FIG. 3: **Theoretical and YBCO 123 linear- T resistivity.** The T dependence of the resistivity $\rho_a(T, 0) = \theta(T - T_c)\rho(T)$ where $\rho(T)$ is given in (1) for the parameter magnitudes of the Table I for YBCO 123 and corresponding experimental curves of Ref.²⁹ for a set of y values. The oxygen content $y - 6$ is obtained from x by use of Fig. 4 (a) of Ref.³⁰. The theoretical T_c is larger at $y = 6.95$ than for $y = 6.85, 7.00$. This is alike in the inset of the second figure. Experimental curves figure from Ref.²⁹.

IV. CONCLUDING REMARKS

That the dependence on the Fermi angle $\phi \in (0, \pi/2)$ of the scattering-rate coefficient $\alpha = \alpha_{\tau_{el}}/\hbar V_F$ associated with that of the inverse lifetime $\hbar/\tau_{el} \approx \hbar\omega\pi\alpha_{\tau_{el}}$ agrees with the experimental points of Fig. 1 seems to confirm the evidence provided in Refs.^{10,12} that the VEPQL may contain some of the main mechanisms behind the unusual properties of the hole-doped cuprates. That in addition the inverse relaxation lifetime $1/\tau$ T -dependence obtained for $\hbar\omega \ll \pi k_B T$ and $x \in (x_A, x_{c2})$ by merely replacing $\hbar\omega$ by $\pi k_B T$ in $1/\tau_{el}$ and averaging over the Fermi line leads to astonishing quantitative agreement with the resistivity experimental lines is a stronger surprising result. Consistently, for $\hbar\omega \ll \pi k_B T$ and $x \in (x_A, x_{c2})$ the system exhibits dynamics characterized by the relaxation time $\tau = \hbar A/\pi k_B T$ of Eq. (A2) of the Appendix A, where $A = [32\sqrt{x x_{op}}/\pi^2] \approx 1$ for $x > x_A$. This second stronger result provides clear evidence of normal-state scale-invariant physics. It may follow from beyond mean-field theory the $T = 0$ line $H_{c2}(x)$, plotted in Fig. S1 for $x \in (x_0, x_{c2})$, referring to a true quantum phase transition. Such a transition could occur between a state with long-range spin order regulated by monopoles and antimonopoles for $H > H_{c2}$ and a vortex liquid by vortices and antivortices for $H < H_{c2}$. That would be a generalization for $H_{c2} > 0$ of the quantum phase transition speculated to occur at $x_{c2} \approx x_0$ and $H_{c2} \approx 0$ in Ref.⁸. The field H^* marks a change from a short-range spin order to a disordered state and thus refers to a crossover. Hence the normal-state scale invariance occurring for $x \in (x_A, x_{c2})$ could result from the hole concentration $x_{c2} \approx 0.2$, where the lines of Fig. S1 associated with the fields $H_{c2}(x)$ and $H^*(x)$ meet, referring to a quantum critical point^{1,2}. Such a quantum critical point may prevent the competing T^2 -quadratic resistivity contribution to strengthen below $x = x_{c2}$.

Acknowledgments

I thank M. A. N. Araújo, J. Chang, A. Damascelli, R. Dias, P. Horsch, S. Komiya, J. Mesot, C. Panagopoulos, T. C. Ribeiro, P. D. Sacramento, M. J. Sampaio, M. Shi and Z. Tešanović for discussions and the support of the ESF Science Program INSTANS and grant PTDC/FIS/64926/2006.

Appendix A: Methods used in our studies

Our general method relies on the use of a suitable description in terms of c and $s1$ fermions whose momenta are close to good quantum numbers of the square-lattice quantum liquids studied in Refs.^{10,12}. The low- T resistivity (1) is accessed for the normal state reached by applying a magnetic field perpendicular to the planes, which remains unaltered down to $T = 0$, as in the cuprates³. The field serves merely to remove superconductivity and achieve the H -independent term $\rho(T)$ of,

$$\rho(T, H) = \rho(T) + \delta\rho(T, H), \quad (\text{A1})$$

where $\delta\rho(T, H)$ is the magnetoresistance contribution. The T -dependent inverse relaxation lifetime derived for finite field, $x \in (x_A, x_{c2})$ and $\hbar\omega \ll \pi k_B T$ by replacing $\hbar\omega$ by $\pi k_B T$ in the one-electron inverse lifetime $\hbar/\tau_{el} \approx \hbar\omega \pi \alpha_{\tau_{el}}$ and averaging over the Fermi line is given by,

$$\frac{1}{\tau(T)} = \frac{2}{\pi} \left(\int_0^{\pi/2} d\phi \frac{1}{\tau_{el}} \right) \Big|_{\hbar\omega=\pi k_B T} = \frac{1}{\hbar A} \pi k_B T, \\ A = \frac{32}{\pi^2} \sqrt{x x_{op}}, \quad x \in (x_A, x_{c2}). \quad (\text{A2})$$

The hole concentration $x_A \approx x_*/2$ is that at which $A \approx 0.5$ becomes of order one. The normal-state resistivity H -independent term $\rho(T)$ of Eq. (A1) then reads,

$$\rho(T) \approx \left(\frac{m_c^\rho d_{||}}{x e^2} \right) \frac{1}{\tau(T)}; \quad m_c^\rho = \frac{\hbar^2 \pi x_*}{2t}, \quad (\text{A3})$$

where m_c^ρ is the c fermion transport mass¹⁰. Combination of Eqs. (A2) and (A3) leads to the resistivity expression given in Eq. (1).

The method used in Ref.¹¹ to derive the one-electron inverse lifetime $1/\tau_{el}$ appearing in the inverse relaxation lifetime of Eq. (A2) is only valid for the hole concentration range $x \in (x_A, x_{c2})$ for which $r_\Delta = V_{Bs1}^\Delta/V_{Fc} \ll 1$. Indeed, for $x \in (x_c, x_A)$ the velocity ratio r_Δ becomes too large. As a result the simple form given in Ref.¹¹ for the matrix element absolute value $|W_{c,s1}(\vec{q}^h, \vec{q}; \vec{p})|$ of the c - $s1$ fermion effective interaction between the initial and final states is not anymore a good approximation. Consistently with the experimental resistivity curves of Fig. 2, the non-linear T dependence of the resistivity developing for approximately $x < x_A$ for a range of low temperatures that increases upon decreasing x is in part due to the increasingly strong effects of the $s1$ fermion boundary-line velocity anisotropy. Our method does not apply to that regime. In turn, for the present range $x \in (x_A, x_{c2})$ the interplay of the c Fermi line isotropy and $s1$ boundary line d -wave like anisotropy^{10,12} also plays an important role. It is behind the c - $s1$ fermion inelastic collisions leading to anisotropic one-electron scattering properties associated with the factor $(\cos 2\phi)^2$ in the above one-electron scattering rate expression.

The linear upper magnetic field $H_{c2}(x)$ line plotted in Refs.^{11,12} for $x \in (x_0, x_{c2})$ is for $x \in (x_0, x_{c1})$ derived in Ref.¹² by means of a method introduced in Ref.⁸. Here $x_0 \approx 0.013$, $x_{c1} = 1/8$ and $x_{c2} \approx 0.20$. However, for $x \in (x_1, x_{c2})$ the actual $H_{c2}(x)$ line may (or may not) slightly deviate to below the straight line plotted in the figure. If so, the hole concentration $x_{c2} \approx 0.20$ may increase to $\approx 0.21 - 0.22$. Fortunately, such a possible deviation does not change the physics discussed in this letter.

¹ Panagopoulos, C. *et al.* Evidence for a generic quantum transition in high- T_c cuprates. *Phys. Rev. B* **66**, 064501 (2002).

² van der Marel, D. *et al.* Quantum critical behaviour in a high- T_c superconductor. *Nature* **425**, 271–274 (2003).

³ Daou, R. *et al.* Linear temperature dependence of resistivity and change in the Fermi surface at the pseudogap critical point of a high- T_c superconductor. *Nature Phys.* **5**, 31–34 (2009).

⁴ Cooper, R. A. *et al.* Anomalous criticality in the electrical resistivity of $\text{La}_{2-x}\text{Sr}_x\text{CuO}_4$. *Science* **323**, 603–607 (2009).

⁵ Jaramillo, R. *et al.* Breakdown of the Bardeen-Cooper-Schrieffer ground state at a quantum phase transition. *Nature* **459**, 405–409 (2009).

⁶ Damascelli, A., Hussain, Z. & Shen, X. Z. Angle-resolved photoemission studies of the cuprate superconductors. *Rev. Mod. Phys.* **75**, 473–541 (2003).

⁷ Lee, P. A., Nagaosa, N. & Wen, X.-G. Doping a Mott insulator: Physics of high-temperature superconductivity. *Rev. Mod. Phys.* **78**, 17–85 (2006).

⁸ Tešanović, Z. d -wave duality and its reflections in high-temperature superconductors. *Nature Phys.* **4**, 408–414 (2008).

⁹ Hübner, S., Hussain, M. A., Damascelli, A. & Sawatzky, G. A. Two gaps make a high temperature superconductor. *Rep. Prog. Phys.* **71**, 062501 (2008).

¹⁰ Carmelo, J. M. P. The square-lattice quantum liquid of charge c fermions and spin-neutral two-spinon $s1$ fermions.

- Nucl. Phys. B* **824**, 452–538 (2010).
- ¹¹ Carmelo, J. M. P. Quantum criticality and correlations in the cuprate superconductors. Supplementary Information. Preprint at (arXiv:1004.1164) (2010).
 - ¹² Carmelo, J. M. P. *d*-wave superconductivity in the virtual-electron pair quantum liquid. Preprint at (arXiv:1004.0923) (2010).
 - ¹³ Yu, G., Li, Y., Motoyama, E. M. & Greven, M. A universal relationship between magnetic resonance and superconducting gap in unconventional superconductors. *Nature Phys.* **5** 873–875 (2009).
 - ¹⁴ Meng, J. *et al.* Coexisting of Fermi arcs and Fermi pockets in a high- T_c copper oxide superconductor. *Nature* **462**, 335–338 (2009).
 - ¹⁵ Vishik, I. M. *et al.* A momentum-dependent perspective on quasiparticle interference in $\text{Bi}_2\text{Sr}_2\text{CaCu}_2\text{O}_{8+\delta}$. *Nature Phys.* **5**, 718–721 (2009).
 - ¹⁶ Xu, G., Gu, G. D., Hücker, M., Fauqué, B., Perring, T. G. & Regnault, L. P. Testing the itinerancy of spin dynamics in superconducting $\text{Bi}_2\text{Sr}_2\text{CaCu}_2\text{O}_{8+\delta}$. *Nature Phys.* **5**, 718–721 (2009).
 - ¹⁷ Kohsaka, Y. *et al.* How Cooper pairs vanish approaching the Mott insulator in $\text{Bi}_2\text{Sr}_2\text{CaCu}_2\text{O}_{8+\delta}$. *Nature Phys.* **5**, 642–646 (2009).
 - ¹⁸ Bergeal, N., Lesueur, J., Aprili, M., Faini, G., Contour, J. P. & Leridon, B. Pairing fluctuations in the pseudogap state of copper-oxide superconductors probed by Josephson effect. *Nature Phys.* **4**, 608–611 (2008).
 - ¹⁹ Sebastian, S. E. *et al.* A multi-component Fermi surface in the vortex state of an underdoped high- T_c superconductor. *Nature* **454**, 200–203 (2008).
 - ²⁰ Chang, J. *et al.* Anisotropic quasiparticle scattering rates in slightly underdoped to optimally doped high-temperature $\text{La}_{2-x}\text{Sr}_x\text{CuO}_4$ superconductors. *Phys. Rev. B* **78**, 205103 (2008).
 - ²¹ Boyer, M. C. *et al.* Imaging the two gaps of the high-temperature superconductor in $\text{Bi}_2\text{Sr}_2\text{CuO}_{6+x}$. *Nature Phys.* **3**, 802–806 (2007).
 - ²² Li, L., Checkelsky, J. G., Komiya, S., Ando, Y. & Ong, N. P. Low-temperature vortex liquid in $\text{La}_{2-x}\text{Sr}_x\text{CuO}_4$. *Nature Phys.* **3**, 311–314 (2007).
 - ²³ Chang, J. *et al.* When low- and high-energy electronic responses meet in cuprate superconductors. *Phys. Rev. B* **75**, 224508 (2007).
 - ²⁴ Tanaka, K. *et al.* Distinct Fermi-momentum-dependent energy gaps in deeply underdoped $\text{Bi}2212$. *Science* **314**, 1910–1913 (2006).
 - ²⁵ Le Tacon, M. *et al.* Two energy scales and two distinct quasiparticle dynamics in the superconducting state of underdoped cuprates. *Nature Phys.* **2**, 537–543 (2006).
 - ²⁶ Abdel-Jawad, M. *et al.* Anisotropic scattering and anomalous normal-state transport in a high-temperature superconductor. *Nature Phys.* **2**, 821–825 (2006).
 - ²⁷ Pines, D. & Nozières, P. in *The theory of quantum liquids* (Benjamin, New York, 1996) Volume 1.
 - ²⁸ Komiya, S., Chen, H.-D., Zhang, S.-C. & Ando, Y. Magic doping fractions for high-temperature superconductors. *Phys. Rev. Lett.* **94**, 207004 (2005).
 - ²⁹ Segawa, K. & Ando, Y. Transport anomalies and the role of pseudogap in the 60-K phase of $\text{YBa}_2\text{Cu}_3\text{O}_{7-\delta}$. *Phys. Rev. Lett.* **86**, 4907–4910 (2001).
 - ³⁰ Liang, R., Bonn, D. A. & Hardy, W. N. Evaluation of CuO_2 plane hole doping in $\text{YBa}_2\text{Cu}_3\text{O}_{6+x}$ single crystals. *Phys. Rev. B* **73**, 180505 (2006).